J Mater Sci: Mater Med (2008) 19:3071–3080
DOI 10.1007/s10856-008-3445-y

Ultrasonic monitoring of foamed polymeric tissue scaffold fabrication

Melissa L. Mather · John A. Crowe · Stephen P. Morgan · Lisa J. White · Alexander N. Kalashnikov · Vladimir G. Ivchenko · Steven M. Howdle · Kevin M. Shakesheff

Received: 25 February 2008 / Accepted: 19 March 2008 / Published online: 5 April 2008

Abstract Polymeric tissue scaffolds are central to many regenerative medicine therapies offering a new approach to medicine. As the number of these regenerative therapies increases there is a pressing need for an improved understanding of the methods of scaffold fabrication. Of the many approaches to processing scaffolds, supercritical fluid fabrication methods have a distinct advantage over other techniques as they do not require the use of organic solvents, elevated processing temperatures or leaching processes. The work presented here is centred on the development of a new approach to monitoring supercritical scaffold fabrication based on determination of the scaffold acoustic impedance to inform protocols for scaffold fabrication. The approach taken uses an ultrasonic pulse-echo reflectometer enabling non-invasive monitoring of the supercritical environment on-line. The feasibility of this approach was investigated for two scaffolds of different molecular weight. Acoustic results demonstrate that differences in the physical properties of the two scaffolds could be resolved, particularly during the foaming process which correlated with findings from time-lapsed imaging and micro X-ray computed tomography (μ X-ray CT) images. Thus, this work demonstrates the feasibility of ultrasonic pulse-echo reflectometry to non-invasively study supercritical scaffold fabrication on-line providing a greater understanding of the scaffold fabrication process.

M. L. Mather (✉) · J. A. Crowe · S. P. Morgan · A. N. Kalashnikov · V. G. Ivchenko
School of Electrical and Electronic Engineering, University of Nottingham, University Park, Nottingham, Nottinghamshire NG7 2RD, UK
e-mail: melissa.mather@nottingham.ac.uk

L. J. White · K. M. Shakesheff
School of Pharmacy, University of Nottingham, University Park, Nottingham, Nottinghamshire NG7 2RD, UK

S. M. Howdle
School of Chemistry, University of Nottingham, University Park, Nottingham, Nottinghamshire NG7 2RD, UK

1 Introduction

Regenerative medicine offers a new approach to medicine which aims to develop biological substitutes that restore, maintain or improve tissue function. The therapeutic strategies for regenerative medicine are well defined and typically involve the culturing of cells from a patient or donor within suitable vessels and/or the guidance of cell growth in three dimensions (3D) via the use of a tissue scaffold [1, 2]. Regenerative medicine has shown early success as demonstrated by the rapid expansion in the number of regenerative therapies currently available, with many more in clinical development. These have primarily targeted the treatment of diabetes, cartilage defects and repair, skin and wound care as well as bone defects [3]. As more and more regenerative medicines reach the market place there is a pressing need for an improved understanding and greater control of the methods of fabrication [2–4]. One such area is in the fabrication of robust and reproducible tissue scaffolds.

Tissue scaffolds are integral to many regenerative therapies, particularly those that promote tissue regeneration via the guidance of cellular growth in 3D [1]. In practice, such scaffolds can either be directly implanted into a patient to act as a space filling, support structure to assist in vivo tissue repair, or used as a structure to guide in vitro tissue growth prior to implantation. Scaffolds are typically designed from bio-mimetic materials which

provide microenvironments for cell–matrix interactions that attempt to mimic biological environments. Candidate scaffold materials include synthetic materials [5, 6], such as polylactic acid (PLA) and poly-lactic-co-glycolic acid (PLGA), and natural materials [7], such as collagen and fibrin. Key advantages to these materials are their biocompatibility, biodegradability and ability to be processed into 3D structures [8–10].

There are many approaches to processing 3D scaffold structures, the chosen method impacting significantly on overall scaffold performance. Processing methods need to produce a structure that is: ideally highly porous ($\sim$80% to 90% depending on sight of implantation [11, 12]); has a network of interconnected pores; has a suitable surface chemistry for cell attachment; and mechanical integrity to match the in vivo environment [8–10]. Current methods of scaffold fabrication include: solvent casting/particulate leaching [13]; emulsification/freeze drying [14]; textile technologies to produce polymer fibres and meshes [15]; gas foaming [16]; liquid–liquid phase separation [17]; and supercritical fluid fabrication methods [6, 8]. In addition to processing suitably structured scaffolds there is a growing interest in developing scaffolds capable of releasing tissue inducing substances such as growth factors [1]. In terms of polymer processing, incorporating bioactive species in scaffolds whilst maintaining the species activity is a significant challenge. The problems associated with this have been previously documented [6, 18] and include difficulties in maintaining protein conformation and activity due to the presence of organic/aqueous solvents (e.g. double emulsion particle formation) and maintaining functionality once exposed to elevated temperatures (e.g. polymer melt processing). In this instance, supercritical fluid fabrication methods have a distinct advantage over other techniques as they do not require the use of organic solvents, elevated processing temperatures or leaching processes, thus enabling bioactive species to be integrated safely into the polymer during the fabrication process [6, 8, 19–21].

A number of approaches to scaffold fabrication using supercritical processes have been demonstrated; with a single step supercritical carbon dioxide ($scCO_2$) foaming process [6, 8] being of particular note. In this instance, $scCO_2$ acts as a plasticizer and foaming agent owing to its gas-like diffusivity and liquid like density. The scaffold fabrication process involves application of $scCO_2$ under high pressure to a polymer powder until a gas saturated state is reached. When depressurised, the gas escapes from the polymer causing it to foam resulting in the formation of a vitrified, porous scaffold. Using this approach, there is potential to tailor the final scaffold characteristics as these depend on the scaffold processing parameters, polymer composition and molecular weight [22]. The relationship between these parameters and final scaffold properties, however, is complex and is currently being investigated [22]. This includes work centred on the implementation of monitoring methods, in-process, to obtain a greater understanding of the effect the supercritical fabrication protocol has on scaffold properties with the aim to obtain improved control in scaffold fabrication.

Monitoring in a high pressure supercritical fluid environment is a challenging task particularly due to the high solubility of supercritical conditions. Due to this, techniques that interrogate the contents of a reaction chamber externally and non-invasively have been investigated. In the past non-invasive characterisation of the size and shape of polymer chains in supercritical conditions has been carried out using small angle X-ray scattering (SAXS) [23] and small angle neutron scattering (SANS) [24]. The availability of such methods, however, is limited. As an alternative, techniques based on the scattering of light have been used to characterise polymer structure in supercritical conditions [25–30], the most successful approaches being those that involve the study of light scattering over multiple angles. Although these approaches are useful they do require purpose built reaction chambers with multiple windows for light transmission and detection [25, 26, 28, 30]. This is not an ideal solution and a more acceptable approach would be to integrate monitoring methods into existing reaction chambers.

This paper presents a new approach to monitoring supercritical scaffold fabrication based on determination of the scaffold acoustic impedance. The approach taken uses an ultrasonic pulse-echo reflectometer for impedance measurements that can be readily integrated into current reaction chamber designs. Further, the reflection geometry used overcomes sound transmission difficulties associated with high sound attenuation both near the critical point [31] and in foamed materials [32, 33]. The overall objective of this work is to demonstrate the feasibility of non-invasive monitoring of supercritical scaffold fabrication in-process using an ultrasonic pulse-echo reflectometer.

2 Materials and methods

2.1 Scaffold materials and fabrication

Scaffolds were fabricated from granules of poly(D,L-lactic acid) ($P_{DL}LA$) (Purac Biomaterials, The Netherlands). Two different scaffold structures were fabricated, one from polymer of average molecular weight 15 kDa and the other from polymer of average molecular weight 52 kDa. Scaffold fabrication was carried out using $scCO_2$ in an in-house designed 100 ml clamp sealed stainless steel high-pressure autoclave [34]. The scaffolds themselves were formed individually inside the autoclave in an in-house designed

rectangular Teflon mould with a detachable tray to allow easy removal of the scaffold after fabrication (see Fig. 1). The mould was attached to a stainless steel ultrasonic delay rod (see Fig. 1), which replaced a window of the high pressure autoclave. Thus, this design could be readily integrated into any reaction vessel with a viewing window. For each study, 160 mg of polymer was added to the mould.

The autoclave was equipped with a pressure transducer and a heating jacket with a CAL 3300 temperature controller (CAL Controls Ltd., UK). High pressure valves (High Pressure Equipment Company, USA), tubing (Swagelok, UK) and fittings (Swagelok, UK) were applied to connect the system. A high pressure PM101 pump (New Ways of Analytics, Germany) was used to charge carbon dioxide (CO_2) into the autoclave. The vessel was heated to 35°C and then pressurized to 230 bar over a period of 20 min. The polymer/CO_2 mixture was then maintained at 35°C and 230 bar for a soaking time of 60 min. Following this, the vessel was depressurized to ambient pressure over a period of 45 min. Throughout the fabrication process the autoclave pressure was computer controlled through the use of a backpressure regulator (BPR, Bronkhorst, Netherlands).

2.2 Ultrasonic pulse-echo reflectometer

The principle of material characterisation based on ultrasonic pulse-echo reflectometery has been previously described [32, 33, 35] and is centred on determination of material acoustic impedance. In practice, acoustic impedance is determined from measurement of the reflection coefficient at an interface between a well characterised material and a material of unknown acoustic properties. For a travelling wave normally incident at an interface, the reflection coefficient (R) is given by:

$$R = \frac{Z_0 - Z_1}{Z_0 + Z_1} \tag{1}$$

where Z_0 is the acoustic impedance (S.I. units of kg m^{-2} s^{-1}) of the well characterised material and Z_1 is the acoustic impedance of the uncharacterised material. Thus, from this equation, the impedance of the uncharacterised material can be found via knowledge of Z_0 and measurement of the reflection coefficient, R.

The measurement scheme for impedance determination used in this work is shown in Fig. 2. Direct measurement of the reflection coefficient is difficult as this requires knowledge of the transducer amplitude response, coupling and radiation response as well as the response of the ultrasound generating electronics. Therefore, in this work the reflection coefficient was determined indirectly through measurement of the first, S_1, and second, S_2, received echoes from the delay rod/sample interface:

$$S_1(\omega) = H(\omega)R_1X(\omega) \tag{2}$$

$$S_2(\omega) = H(\omega)R_0R_1^2X(\omega)^2 \tag{3}$$

where $H(\omega)$ is the combined response of the transducer and ultrasonic generating electronics, R_0 is the reflection

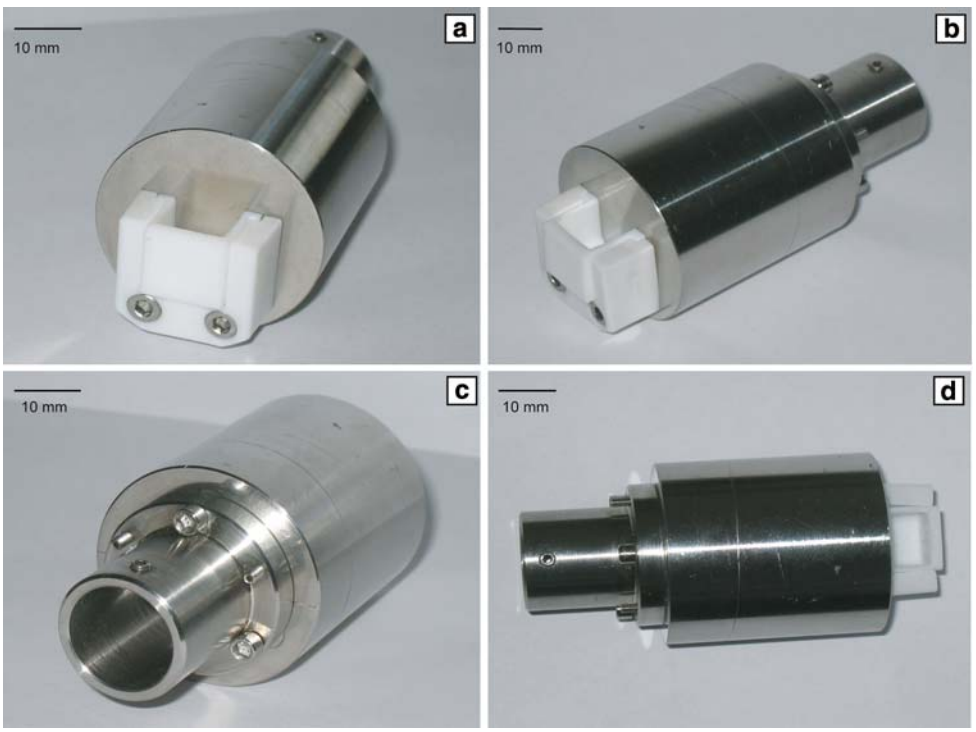

Fig. 1 Pulse-echo reflectometer apparatus consisting of a stainless steel delay rod, transducer clamp and sample holder. (**a**) Front view showing sample holder, (**b**) side view showing sample holder, (**c**) side view showing transducer clamp, (**d**) top view

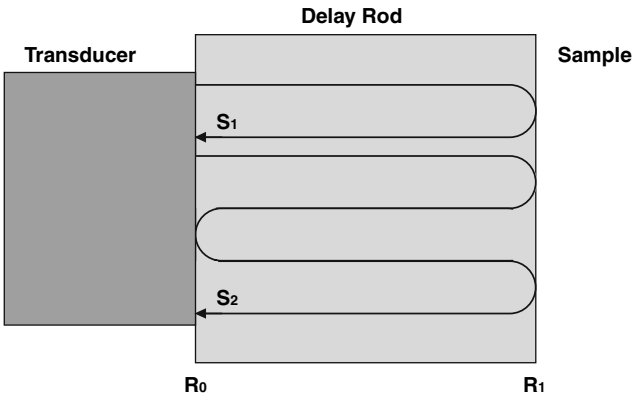

Fig. 2 Acoustic signal propagation path. S_1 is the first reflected signal from the delay rod-sample interface, S_2 is the second reflected signal whilst R_0 and R_1 are the reflection coefficients at the transducer-delay rod and delay rod-sample interfaces, respectively

coefficient at the delay rod/transducer interface, R_1 is the reflection coefficient at the delay rod/sample interface, $X(\omega)$ is the response of the delay rod and ω is the angular frequency of the ultrasonic signal. By taking the quotient, M, of (3) and (2), the need to measure the system response, $H(\omega)$, is removed and:

$$M(\omega) = R_0 R_1 X(\omega) \tag{4}$$

To remove the need to directly measure R_0 and $X(\omega)$, the system was calibrated with air. The acoustic properties of air are well documented. In particular, the acoustic impedance of air is negligible compared to the stainless steel delay rod, thus, the reflection coefficient in this instance is ≈ 1 and (4) becomes:

$$M_{\text{air}}(\omega) = R_0 X(\omega) \tag{5}$$

Therefore, the reflection coefficient of a sample of unknown properties can be determined from a ratio of the (4) and (5):

$$R_1 = \frac{M_{\text{sample}}}{M_{\text{air}}} \tag{6}$$

Once R_1 has been determined Z_1 can be calculated using the known impedance of the delay rod.

2.3 Ultrasonic experimental systems

The experimental ultrasonic pulse-echo reflectometer consisted of an ultrasonic transducer (Panametrics Inc., Waltham, USA) clamped to a stainless steel delay rod ($Z = 45.7 \times 10^6$ kg m^{-2} s^{-1}) and coupled with ultrasonic coupling gel. The delay rod clamp was co-axial with the transducer and had sufficient adjustability to ensure that good coupling was maintained throughout measurements. Also, the central axis of the transducer was co-incident with the mid-point of the Teflon mould used to form the scaffolds, (see Fig. 1). The transducer had a centre frequency of 20 MHz and was used in pulse-echo mode. Additionally, an ultrasonic pulser-receiver and self-calibrating scalable research platform [36], as an ultrasonic back end, were used. The pulser was excited from the platform in order to minimize frame jitter [37], and provided a 100 V rectangular pulse with a duration of approximately 25 ns. The received echoes (S_1 and S_2) were amplified to utilise the full input range of the analogue to digital converter (ADC) on the platform. The platform employed both averaging and accurate interleaved sampling in order to increase the accuracy of the acquired ultrasonic records by using their repeated excitation [38]. The records were averaged 1,024 times each, and the equivalent sampling frequency was multiplied by a factor of 27 compared to the ADC sampling frequency. This required 5.5 s for a single record to be acquired at a pulse repetition frequency of 5 kHz. New acquisitions started every 10 s, and the records were written to a computer file for offline processing. Two acquisition windows were used in order to acquire S_1 and S_2, respectively. The received signals were analysed off-line to determine R and Z as a function of time throughout the scaffold fabrication process.

2.4 Ultrasonic simulation in supercritical conditions

For validation of the acoustic impedance measured using the ultrasonic pulse-echo reflectometer, simulations were carried out to predict the change in CO_2 acoustic impedance during fabrication. CO_2 was chosen for validation purposes rather than the polymer samples as its phase behaviour is less complex. Simulations were centred on determination of the thermophysical properties of CO_2 using the thermodynamic equation of state which, were then used to derive the acoustic impedance, Z:

$$Z = \rho c \tag{7}$$

where ρ is density and c is the speed of sound, both of which are dependent on the thermophysical properties of the material of propagation:

$$\rho = \frac{MW}{V} \tag{8}$$

$$c = \sqrt{\frac{\gamma B}{\rho}} \tag{9}$$

where MW is molecular weight, V is molar volume, γ is the ratio of specific heats and B is the isothermal bulk modulus given by:

$$B = -V\frac{\partial P}{\partial V_T} \tag{10}$$

where P is pressure and T is temperature. In practice, a cubic form of the equation of state was chosen to predict

thermophysical properties due to its simplicity of solution and its capability to describe the phase behaviour in supercritical fluids [39]. The form of this equation is given by:

$$X^3 + \alpha X^2 + \beta X + \gamma = 0 \quad (11)$$

where $X = PV/RT$, R is the universal gas constant, and α, β and γ are the equation of state constants [40]. In this work the Peng–Robinson–Gasem cubic equation of state was chosen as it only requires three input parameters and describes the temperature dependence of pressure and volume better than many other cubic formulations [41]. The exact form of α, β and γ are described elsewhere [41]. Initially Eq. 11 was solved and the location of phase boundaries and molar volume for given temperature–pressure pairs determined. Through knowledge of the molar volume the density was calculated using (8) and from the partial derivative of pressure with respect to volume the bulk modulus determined using (10). The equipartition theory of specific heats was used to predict the variation of γ with temperature using a Maxwell–Boltzmann distribution of molecular energies. For the purposes of simplicity, pressure variation was not incorporated in the description of γ.

2.5 Time-lapsed optical imaging

To assist in interpretation of ultrasonic measurements time-lapsed optical imaging of scaffold fabrication was employed. In this instance, the ultrasonic delay rod was replaced with a sapphire window and the scaffold fabrication process repeated. The scaffold sample was illuminated via a back window in the reaction chamber via a white light emitting diode (LED) and a diffuser to provide close to uniform illumination across the viewing window. Front illumination, provided by a circular array of white LEDs, and image capture were applied through the front window. For image capture a charge coupled device (CCD) camera (uEye, IDS Imaging, Germany) with a video zoom lens was used. The camera was connected to a computer via a USB 2.0 interface. An in-house standalone program was written in MATLAB® to control image capture. Images were captured at 2 s intervals throughout the fabrication process and written to a computer file for off-line analysis.

2.6 Post-fabrication scaffold characterisation

Scaffolds were characterised post-fabrication using μ X-ray CT. The use of μ X-ray CT to characterise scaffolds is well documented [10, 42–46]. In this work μ X-ray CT images of scaffolds were obtained using a high resolution μ-CT system (Skyscan 1174 compact CT, Skyscan, Belgium). Scaffolds were mounted on a stage within the imaging system and subsequently scanned. The scanner was set to a voltage of 34 kV and a current of 800 μA; the resolution was 16 μm. The resulting 16 bit, 2D images were saved using the tagged image file format (tiff).

3 Results and discussion

Figure 3 displays the reflection coefficient as a function of time for the case of no polymer (i.e. CO_2), the $P_{DL}LA$ 15 kDa sample and the $P_{DL}LA$ 52 kDa sample. The graph also indicates the critical point during filling and venting as well as the pressure profile describing the pressure applied to the reaction chamber throughout the process. The non-linearity in the pressure profile during the venting stage is due to instability in the backpressure regulator. Comparison of the three curves tracking the reflection coefficient and the pressure profile indicates that the three phases of the scaffold fabrication process (filling, soaking and venting) can be identified from measurement of the reflection coefficient. In general, during the filling stage the reflection coefficient undergoes considerable change. During the soaking stage the reflection coefficient is relatively more stable whilst during the venting stage large variations in the reflection coefficient are observed. Also of note are the stationary points observed for each reflection curve near the critical point during filling and venting. These observations demonstrate the sensitivity of the reflection coefficient to changes in phase and physical properties of the sample under investigation.

The relative magnitude of the reflection coefficient shown in Fig. 3 for the samples studied is also of interest. In particular, the reflection coefficient is highest for the

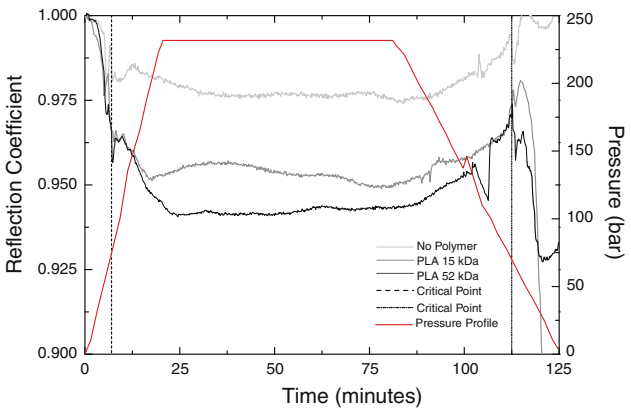

Fig. 3 Reflection coefficient as a function of scaffold fabrication time. The curves show results for the case of no polymer, $P_{DL}LA$ 15 kDa sample and $P_{DL}LA$ 52 kDa sample as well as the location of the critical point during filling and venting. The pressure profile as monitored by the back pressure regulator is also shown

case of no polymer where the reflection occurs at an interface between the delay rod and CO_2 in the reaction vessel. In this instance, observed changes in the reflection coefficient are correlated with changes in the phase and physical properties of CO_2 such as the increase in density of $scCO_2$ compared to gaseous CO_2. Differences in the reflection for the case of $P_{DL}LA$ 15 kDa and $P_{DL}LA$ 52 kDa polymers are also seen. Again these are due to differences in the physical properties of these polymers. For example, the lower reflection coefficient observed for $P_{DL}LA$ 52 kDa, compared to $P_{DL}LA$ 15 kDa during the filling stage, can be related to both its higher density and viscosity. Further, the observed reduction in reflection for both polymers following plasticization by the supercritical process can be associated with an increase in polymer density from their initial loosely packed form to a liquid-like state. Differences in reflection coefficient of the two polymers during the venting stage are also observed. These differences may be due to the molecular weight dependence of foaming with the higher molecular weight $P_{DL}LA$ 52 kDa polymer tending to entangle more than $P_{DL}LA$ 15 kDa and in doing so lock in CO_2 whilst the lower molecular weight $P_{DL}LA$ 15 kDa polymer enables an easier escape for the CO_2, resulting in rapid foam formation with larger pores [22].

Further insight into changes in sample acoustic properties throughout the scaffold fabrication process can be gained through inspection of Fig. 4 that displays results of acoustic impedance determined from measurement for all samples and from simulation for the case of CO_2. As a reference the critical point is marked during filling and venting along with the pressure profile. From inspection of Fig. 4 it can be seen that the measured impedance of CO_2 is comparable with simulated results, the differences between the two curves to be expected due to both errors in the experimental measurements and inadequacies in the equation of state to sufficiently describe the phase changes occurring, particularly around the critical point. As expected the acoustic impedance determined for both polymer samples is greater than that determined for CO_2 with $P_{DL}LA$ 52 kDa having the higher impedance of the two polymers studied during the filling stage. During the venting stage the rate of change of acoustic impedance is different for the two polymers and may be indicative of different foaming rates. The magnitude of the acoustic impedance found for both polymers is comparable to the literature values of polystyrene (2.5×10^6 kg m^{-2} s^{-1}) [47], which is known to have similar physical properties to PLA [48]. An unexpected observation, however, was the higher final value of acoustic impedance for the $P_{DL}LA$ 15 kDa sample compared to the $P_{DL}LA$ 52 kDa sample. This is thought to have arisen due to the formation of a denser skin at the front face of the scaffold during the rapid foaming process. Overall the results found here provide support to the feasibility of tracking changes in scaffold fabrication and physical properties using ultrasonic pulse-echo reflectometry.

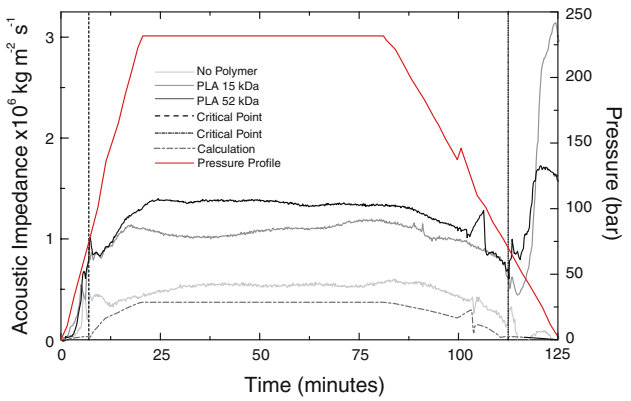

Fig. 4 Acoustic impedance as a function of scaffold fabrication time. The curves show results for the case of no polymer, $P_{DL}LA$ 15 kDa sample, $P_{DL}LA$ 52 kDa sample, the location of the critical point during filling and venting as well as the calculated impedance for the case of no polymer. The pressure profile is also plotted

To provide further insight into the fabrication process and to assist in the interpretation of acoustic results, time-lapsed imaging of scaffold fabrication was carried out, as illustrated in Fig. 5. At each time point shown (a) corresponds to the $P_{DL}LA$ 15 kDa sample and (b) to the $P_{DL}LA$ 52 kDa sample. The main distinctions between the two polymers occur during plasticization and foaming. The lower molecular weight sample, $P_{DL}LA$ 15 kDa, undergoes a greater reduction in volume than the $P_{DL}LA$ 52 kDa following plasticization (Fig. 5 time 4 min and time 7 min). Further, the foaming process for the two polymers is distinct with the $P_{DL}LA$ 15 kDa sample displaying a rapid foaming process during the final 5 min of fabrication whilst the $P_{DL}LA$ 52 kDa sample commences foaming earlier but at a slower rate than $P_{DL}LA$ 15 kDa. This correlates with the interpretation of acoustic impedance results during the foaming process.

The above investigations have demonstrated distinctions between the $P_{DL}LA$ 15 kDa sample and the $P_{DL}LA$ 52 kDa sample during the fabrication process. In order to determine if these distinctions persist post-fabrication the samples were imaged using μ X-ray CT, Fig. 6. Images represent cross sections of the scaffolds along the axis parallel to acoustic wave propagation with Fig. 6a, c, e showing cross sectional images of the $P_{DL}LA$ 15 kDa sample and Fig. 6b, d, f of the $P_{DL}LA$ 52 kDa sample. The cross sections of the $P_{DL}LA$ 15 kDa scaffold are smaller than those of the $P_{DL}LA$ 52 kDa sample due to damage caused to the fragile $P_{DL}LA$ 15 kDa sample on removal from the sample holder. Inspection of the images in Fig. 6 reveals structural differences in the samples. These differences were quantified (see Table 1) using the SkyScan

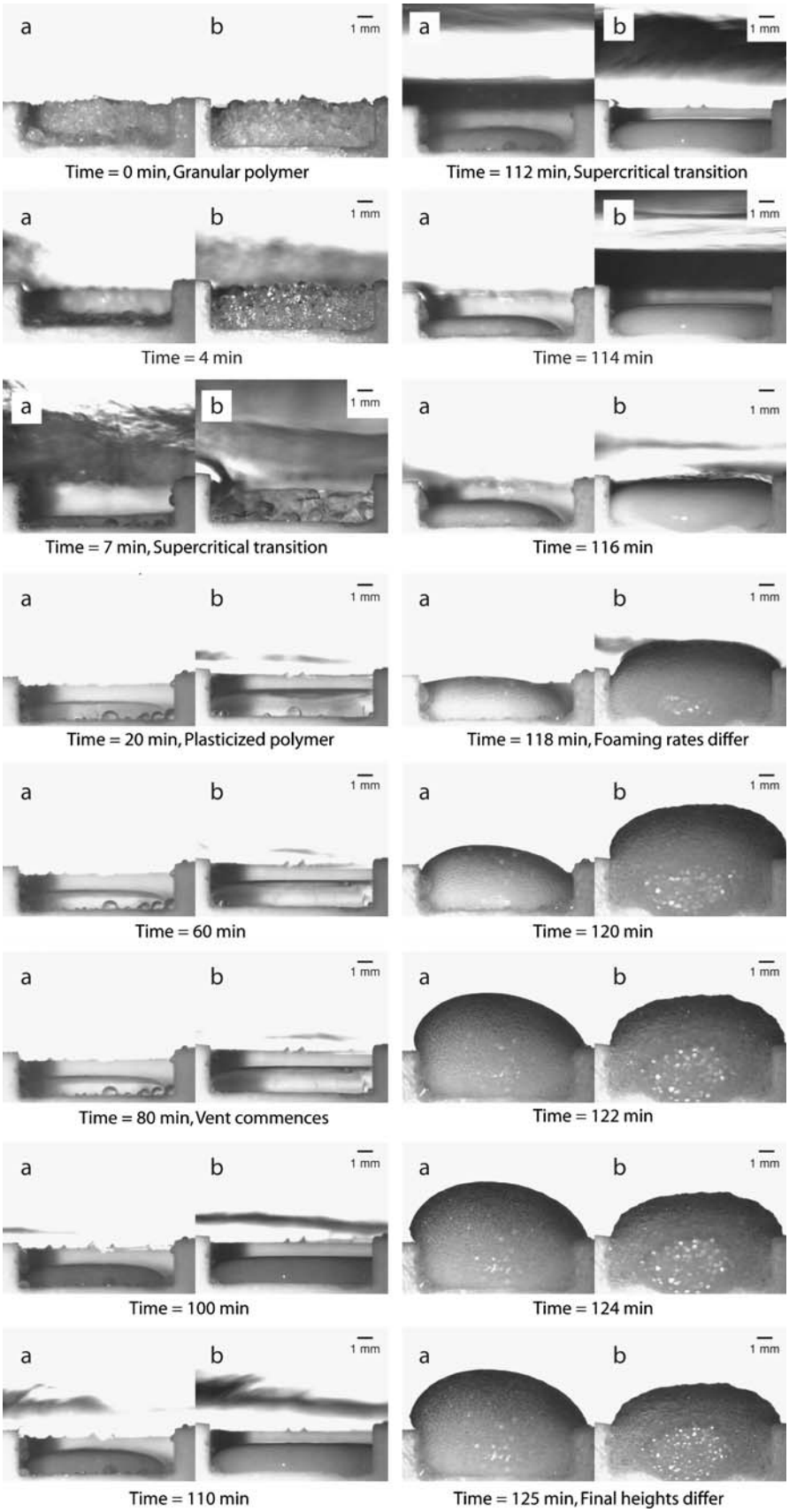

Fig. 5 Time-lapsed imaging of the scaffold fabrication process. At each time point shown (**a**) corresponds to the $P_{DL}LA$ 15 kDa sample and (**b**) to the $P_{DL}LA$ 52 kDa sample

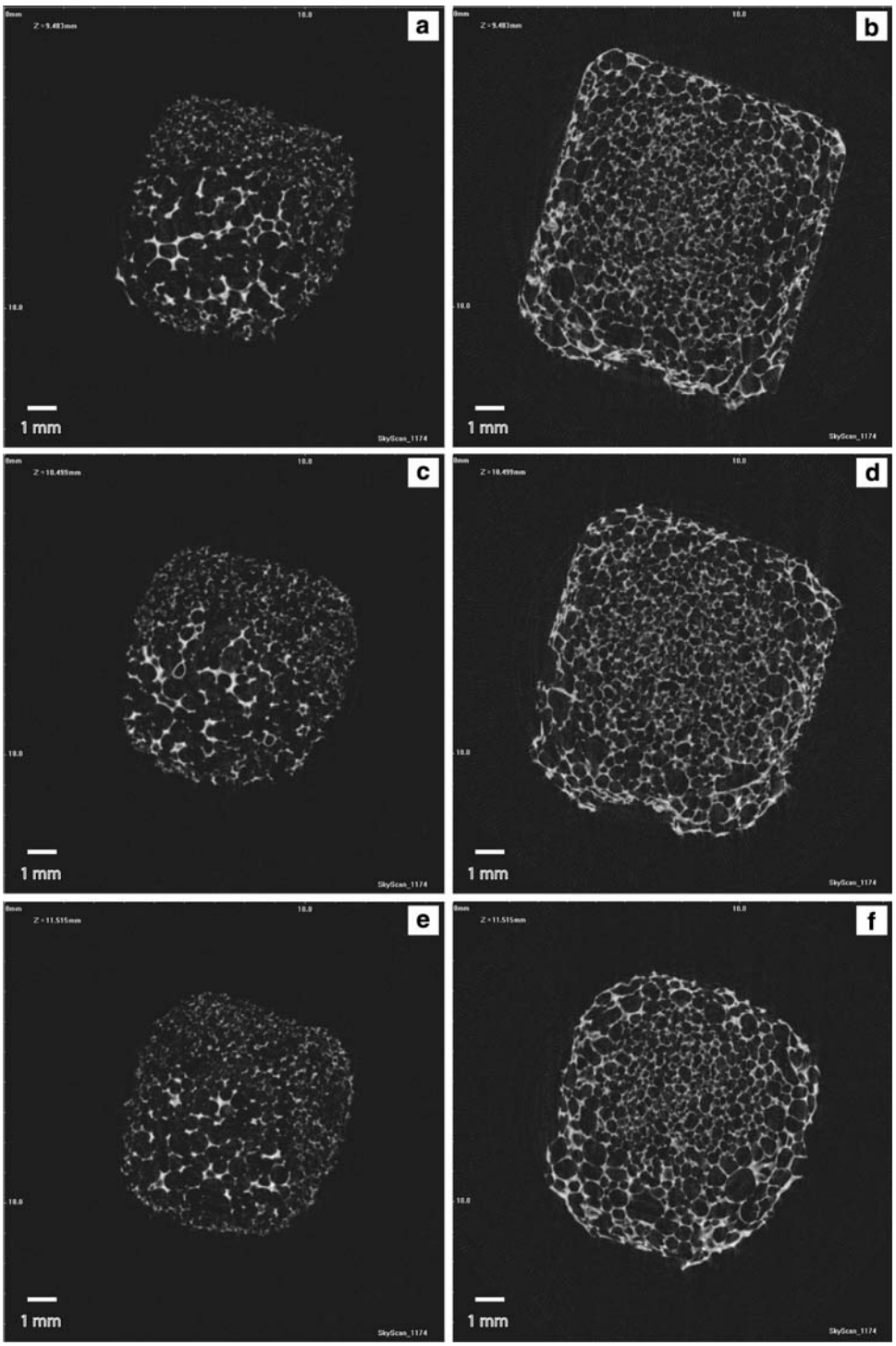

Fig. 6 μ X-ray CT images of scaffolds post-fabrication. (**a**, **c**, **e**) Are cross sections of the $P_{DL}LA$ 15 kDa sample and (**b**, **d**, **f**) are of the $P_{DL}LA$ 52 kDa sample

Table 1 Scaffold porosity and pore size properties as calculated using SkyScan Analyser software (version 1.6.1.1)

	$P_{DL}LA$ 15 kDa	$P_{DL}LA$ 52 kDa
Porosity (%)	83	72
Mean pore size (μm)	430	330

Analyser Software (version 1.6.1.1 SkyScan) with global thresholding, image pre-smoothing and upper and lower greyscale threshold values set to 40 and 255, respectively. These results provide further support that the distinctions found in measured acoustic properties are related to physical differences in the polymer samples.

4 Conclusion

This work has presented a new application of ultrasonic pulse-echo reflectometry to monitoring supercritical scaffold fabrication. A key advantage of this approach is the ability to non-invasively monitor the supercritical environment on-line. Further, minimal modification to existing reaction vessels used for scaffold fabrication is required for integration of the ultrasonic pulse-echo reflectometer system and the reflection geometry used overcomes sound transmission difficulties associated with high sound attenuation near the critical point [31] and in foamed materials [32, 33]. Initially the measurement system was validated through comparison of experimental values of acoustic impedance for CO_2 with simulated values as calculated using the Peng–Robinson–Gasem equation of state. Measured and predicted values were comparable. Next, the feasibility of non-invasive monitoring of the supercritical scaffold fabrication process was demonstrated for two polymer samples: $P_{DL}LA$ 15 kDa and $P_{DL}LA$ 52 kDa. Through measurement of the reflection coefficient and determination of the acoustic impedance, the different stages of scaffold fabrication (filling, soaking and venting) were monitored along with changes in the scaffold physical properties. Further, differences in the physical properties of the two scaffolds were resolved, particularly during the foaming process. The differences in the foaming process and physical properties observed acoustically correlated with results from time-lapsed imaging and μ X-ray CT images. It is concluded that ultrasonic pulse-echo reflectometry has promise to be a useful tool to non-invasively study supercritical scaffold fabrication on-line and has the advantage over time-lapsed imaging of quantifying changes in scaffold physical properties in process. It has particular application for the monitoring of scaffold supercritical fabrication processes to provide greater understanding of the effect fabrication protocol has on scaffold properties. Thus, there is potential to extend the application of ultrasonic pulse-echo reflectometry from the food industry [32, 33] to monitor of the mass production of scaffolds. Finally, the work presented here provides the basis for further studies involving a broader range of scaffold compositions and fabrication protocols to assess the robustness of ultrasonic pulse-echo reflectometry for scaffold characterisation.

Acknowledgements The authors wish to acknowledge Prof. Richard Challis for his guidance in acoustic modeling of supercritical conditions. Michael Brion is also acknowledged for his help in obtaining time-lapsed movies of scaffold formation. This work is supported by the Engineering and Physical Sciences Research Council, UK through the 'remedi' project, Grant No. EP/C534247/1.

References

1. R. Langer, J.P. Vacanti, Science **260**, 920 (1993)
2. R. Langer, Tissue Eng. **13**, 1 (2007)
3. L.G. Griffith, G. Naughton, Science **295**, 1009 (2002)
4. R. Archer, D.J. Williams, Nat. Biotechnol. **23**, 1353 (2005)
5. J.S. Tjia, P.V. Moghe, J. Biomed. Mater. Res. **43**, 291 (1998)
6. S.M. Howdle, M.S. Watson, M.J. Whitaker, V.K. Popov, M.C. Davies, F.S. Mandel, J.D. Wang, K.M. Shakesheff, Chem. Commun. **1**, 109 (2001)
7. J.L. Drury, D.J. Mooney, Biomaterials **24**, 4337 (2003)
8. R.A. Quirk, R.M. France, K.M. Shakesheff, S.M. Howdle, Curr. Opin. Solid State Mater. Sci. **8**, 313 (2004)
9. D.W. Hutmacher, Biomaterials **21**, 2529 (2000)
10. G.H. van Lenthe, H. Hagenmuller, M. Bohner, S.J. Hollister, L. Meinel, R. Muller, Biomaterials **28**, 2479 (2007)
11. T.S. Karande, J.L. Ong, C.M. Agrawal, Ann. Biomed. Eng. **32**, 1728 (2004)
12. A.S. Goldstein, G. Zhu, G.E. Morris, R.K. Meszlenyi, A.G. Mikos, Tissue Eng. **5**, 421 (1999)
13. A.G. Mikos, A.J. Thorsen, L.A. Czerwonka, Y. Bao, R. Langer, D.N. Winslow, J.P. Vacanti, Polymer **35**, 1068 (1994)
14. K. Whang, C.H. Thomas, K.E. Healy, G. Nuber, Polymer **36**, 837 (1995)
15. A.G. Mikos, Y. Bao, L.G. Cima, D.E. Ingber, J.P. Vacanti, R. Langer, J. Biomed. Mater. Res. **27**, 183 (1993)
16. Y.S. Nam, J.J. Yoon, T.G. Park, J. Biomed. Mater. Res. **53**, 1 (2000)
17. Y.S. Nam, T.G. Park, J. Biomed. Mater. Res. **47**, 8 (1999)
18. K. Fu, A. Klibanov, R. Langer, Nat. Biotechnol. **18**, 24 (2000)
19. J.J.A. Barry, M. SIlva, V.K. Popov, K.M. Shakesheff, S.M. Howdle, R Soc London Philos. Transact. A Math. Phys. Eng. Sci. **364**, 249 (2006)
20. D.D. Hile, M.L. Amirpour, A. Akgerman, M.V. Pishko, J. Control. Release **66**, 177 (2000)
21. D.J. Mooney, D.F. Baldwin, N.P. Suh, J.P. Vacanti, R. Langer, Biomaterials **17**, 1417 (1996)
22. H. Tai, M.L. Mather, D. Howard, W. Wang, L.J. White, J.A. Crowe, S.P. Morgan, A. Chandra, D.J. Williams, S.M. Howdle, K.M. Shakesheff, Eur. Cells Mater. **14**, 64 (2007)
23. K. Nishikawa, I. Tanaka, J. Phys. Chem. **100**, 418 (1996)
24. G.D. Wignall, J. Phys. Condens. Matter **11**, R157 (1999)
25. S. Zhou, B. Chu, Macromolecules **31**, 5300 (1998)
26. S. Zhou, B. Chu, H.S. Dhadwal, Rev. Sci. Instrum. **69**, 1955 (1998)
27. R.D. Smith, J.L. Fulton, J.P. Blitz, J.M. Tingey, J. Phys. Chem. **94**, 781 (1990)
28. J. Kojima, Y. Nakayama, M. Takenaka, T. Hashimoto, Rev. Sci. Instrum. **66**, 4066 (1995)
29. N. Kuwahara, K. Kubota, Phys. Rev. A **45**, 7385 (1992)
30. Y. Xiong, E. Kiran, Rev. Sci. Instrum. **69**, 1463 (1998)
31. R.M. Oag, P.J. King, C.J. Mellor, M.W. George, J. Ke, M. Poliakoff, V.K. Popov, V.N. Bagratashvili, J. Supercrit. Fluids **30**, 259 (2004)
32. A. Kulmyrzaev, C. Cancelliere, D.J. McClements, J. Food Eng. **46**, 235 (2000)
33. P. Fairley, D.J. McClements, M.J.W. Povey, Proc. Inst. Acoust. **13**, 63 (1991)
34. F. Furno, P. Licence, S.M. Howdle, M. Poliakoff, L'Actualite Chimique **4–5**, 62 (2003)
35. D.J. McClements, P. Fairley, Ultrasonics **29**, 58 (1991)
36. A.N. Kalashnikov, V.G. Ivchenko, R.E. Challis, W. Chen, *Instrumentation and Measurement Technology Conference Proceedings—IEEE* (Warsaw, Poland, 2007), p. 1
37. A.N. Kalashnikov, R.E. Challis, M.U. Unwin, A.K. Holmes, IEEE Trans. Instrum. Meas. **54**, 2177 (2005)

38. A.N. Kalashnikov, V.G. Ivchenko, R.E. Challis, B.R. Hayes-Gill, IEEE Trans. Ultrason. Ferroelectr. Freq. Control **54**, 1596 (2007)
39. J.O. Valderrama, Ind. Eng. Chem. Res. **42**, 1603 (2003)
40. S.I. Sandler, *Chemical and Engineering Thermodynamics* (John Wiley & Sons, New York, 1999)
41. K.A.M. Gasem, W. Gao, Z. Pan, R.L. Robinson Jr., Fluid Phase Equilib. **181**, 113 (2001)
42. S. Cartmell, K. Huynh, A. Lin, S. Nagaraja, R. Guldberg, J. Biomed. Mater. Res. **69A**, 97 (2004)
43. A.L. Darling, W. Sun, J. Biomed. Mater. Res. **70B**, 311 (2004)
44. S.T. Ho, D.W. Hutmacher, Biomaterials **27**, 1362 (2006)
45. J.R. Jones, G. Poologasundarampillai, R.C. Atwood, D. Bernard, P.D. Lee, Biomaterials **28**, 1404 (2007)
46. M.J. Moore, E. Jabbari, E.L. Ritman, L. Lu, B.L. Currier, A.J. Windebank, M.J. Yaszemski, J. Biomed. Mater. Res. **71A**, 258 (2004)
47. G.W.C. Kaye, T.H. Laby, J.G. Noyes, G.F. Phillips, O. Jones, J. Asher, *Tables of Physical and Chemical Constants* (Longman, 1995)
48. A. Mohamed, S.H. Gordon, G. Biresaw, J. Appl. Polym. Sci. **106**, 1689 (2007)